Optical emission related to basal-plane stacking faults in *m*-plane $Zn_{1-x}Mg_xO$ epilayers for $0 \leqslant x \leqslant 0.1$

Wan-Hsien Lin, Pierre Corfdir, Uwe Jahn,* and Holger T. Grahn

Paul-Drude-Institut für Festkörperelektronik, Leibniz-Institut im Forschungsverbund Berlin e. V., Hausvogteiplatz 5–7, 10117 Berlin, Germany

(Received 27 May 2016; revised manuscript received 22 July 2016; published 30 September 2016)

We investigate the optical properties of type-I_1 basal-plane stacking faults (BSFs) in ZnO and $Zn_{1-x}Mg_xO$ by cathodoluminescence spectroscopy supported by envelope function calculations. We report on a quantum-well-like band alignment of the I_1 BSFs in ZnO taking into account the spontaneous polarization as well as an intrinsic self-screening effect on the polarization-related electric field. We present a systematic investigation of the luminescence properties associated with I_1 BSFs in $Zn_{1-x}Mg_xO$ for varying Mg content ($0 \leqslant x \leqslant 0.1$) using spatially and spectrally resolved cathodoluminescence spectroscopy. Both the near-band-edge emission and the luminescence line related to the I_1 BSF exhibit the expected blueshift and line broadening with increasing Mg content. We propose a band diagram to describe the recombination mechanism of excitons in a $Zn_{1-x}Mg_xO$ film containing I_1 BSFs. Based on a statistical analysis, we compile the experimentally obtained I_1 BSF emission energies of $Zn_{1-x}Mg_xO$ samples and establish a linear dependence of the I_1 BSF-related emission energy on the Mg content. This correlation provides an alternative way to identify the presence of I_1 BSFs in $Zn_{1-x}Mg_xO$ without the necessity of sophisticated transmission electron microscopy investigations.

DOI: 10.1103/PhysRevB.94.115209

I. INTRODUCTION

$ZnO/Zn_{1-x}Mg_xO$, a wide-band gap material system exhibiting the hexagonal wurtzite (WZ) structure, has been extensively used for applications, e.g., in photocatalysts [1,2], solar cells [3,4], gas sensors [5], UV photodetectors [6], and light emitting diodes [7]. The energy gap of $Zn_{1-x}Mg_xO$ increases upon an increasing substitution of Zn atoms by Mg atoms [8–11] and shows, according to a recent study by Chia *et al.* [12], a linear dependence on x for values of the Mg content between 0 and 0.12.

Similar to GaN, the existence of both an intrinsic spontaneous and a strain-related piezoelectric polarization induces an internal electric field within $ZnO/Zn_{1-x}Mg_xO$ heterostructures such as quantum wells (QWs) when grown along the polar c-axis. The discontinuity of these fields at the interfaces of the heterostructures induces a quantum-confined Stark effect that is detrimental for the quantum efficiency of optoelectronic devices [13,14]. Therefore, there is a large interest in the growth of nonpolar $ZnO/Zn_{1-x}Mg_xO$ layer structures with $(10\bar{1}0)$ and $(11\bar{2}0)$ orientations [15–19], which are usually referred to as m- and a-plane heterostructures, respectively. However, the growth of nonpolar ZnO is often associated with the formation of basal-plane stacking faults (BSFs) with densities on the order of 10^5 cm^{-1} [20,21]. These extended defects are likely to originate from the coalescence boundaries formed by the three-dimensional nucleation growth mode for a- or m-plane ZnO [22]. A BSF is formed because of a misinsertion of an atomic layer, leading to the fact that the local atomic stacking sequence changes from WZ to zinc blende (ZB), forming a WZ-ZB-WZ intrinsic heterostructure. Among the four types of BSFs in ZnO [23], the type-I_1 BSF exhibits the lowest formation energy leading to its preferential generation during growth. Thus, it is the only one which has been experimentally studied to date.

Only a few reports have presented theoretical [23] and experimental [12,24–32] studies of the luminescence properties associated with I_1 BSFs in ZnO. Using a combined transmission electron microscopy (TEM) [21] and cathodoluminescence (CL) study of an m-plane ZnO epitaxial film [28], we have previously clarified that luminescence lines associated with I_1 BSFs can be observed between 3.310 and 3.335 eV [28]. Although the I_1 BSF-related luminescence line is usually observed at low temperatures, we have demonstrated that it does contribute to the low-energy tail of an asymmetric near-band-edge (NBE) luminescence line even at room temperature [28]. Thus, I_1 BSFs can also have an impact on the luminescence properties of ZnO-based optoelectronic devices.

So far, the actual nature of the BSF-related optical emission of ZnO is still controversial. On the one hand, following the work of Schirra *et al.* [24], this luminescence line has been assigned to a free electron-to-acceptor state transition (e, A^0) [12,24–26,32]. The nature of the I_1 BSF-related acceptor is, however, still unclear. On the other hand, this luminescence line has been assigned to an excitonic transition, where the exciton is bound to an I_1 BSF [23,27–31]. The second interpretation is based on the fact that an I_1 BSF in a wurtzite crystal forms a sequence of WZ-ZB-WZ crystal structures along the c-axis, assuming that the energy gap of the ZB phase is smaller than the one of the WZ phase and/or that the ZB phase exhibits a negative conduction band (CB) offset with respect to the WZ phase. As a result, the I_1 BSF forms an intrinsic QW, in which excitons can be captured, leading to an efficient I_1 BSF-related excitonic emission. For GaN, this QW model has already been proposed some time ago [33,34], and its validity has been experimentally confirmed [35,36]. For ZnO, most authors refer to the type-II band alignment that has been calculated by Yan *et al.* [23]. Following the modeling in Ref. [23], electrons are confined in the ZB QW, and the CB and valence band (VB) offsets between the ZB

*ujahn@pdi-berlin.de

and WZ phases amount to 0.147 and 0.037 eV, respectively. Moreover, the ZB ZnO energy gap is predicted to be 0.110 eV smaller than the one of WZ ZnO (3.434 eV) [29] and thus has a value of 3.324 eV. The energy gap of ZB ZnO derived from the calculations in Ref. [23] is in fairly good agreement with the fact that the NBE luminescence lines of ZB ZnO at low temperatures are centered at 3.28 eV [37] and 3.29 eV [25]. Since the exciton binding energy in ZnO is 60 meV, the energy gap of ZB ZnO at low temperatures is about 3.34–3.35 eV. Consequently, the energy-band alignment of an ideal I_1 BSF can be interpreted as a type-II QW structure, and a QW model seems to be also feasible for the I_1 BSF in ZnO. However, Yan *et al.* [23] predicted a very weak carrier localization at the I_1 BSFs, leading to the conclusion that I_1 BSFs of ZnO are electronically inert, i.e., exhibit a negligible optical activity. This conclusion has to be verified, since the calculations of Ref. [23] do not explicitly take into account the spontaneous polarization of ZnO, which amounts to -0.057 C/m^2 (about two times larger than in GaN) [38] and which should result in a significant band bending across the I_1 BSF-related QW.

The impact of I_1 BSF on the optical properties of the ternary $Zn_{1-x}Mg_xO$ system, which serves, e.g., as a barrier material and/or active layers in optoelectronic devices operating in the UV spectral range, has not yet been systematically investigated. The broadening of the NBE emission lines due to unavoidable composition fluctuations is a serious obstacle in order to resolve I_1 BSF- and NBE-related luminescence lines [39]. Two recent reports on the photoluminescence (PL) properties of $Zn_{1-x}Mg_xO$ films fabricated by molecular-beam epitaxy [40] and sol-gel spin coating [12] have revealed the presence of a defect-related emission peak centered at an energy 50 meV below the energy of the NBE emission (E_{NBE}). This peak was assigned to BSFs based solely on its spectral position with respect to the NBE emission line, and no additional evidence has been reported to prove the connection of this defect-related emission line to I_1 BSFs.

In the present study, we first discuss the QW model of the I_1 BSF in ZnO based on calculations of the corresponding band alignment taking into account the spontaneous polarization of ZnO and an intrinsic self-screening of the polarization-related electric field. For the second part of this work, we utilize spectrally and spatially resolved CL spectroscopy to identify the spatial positions of I_1 BSFs in $Zn_{1-x}Mg_xO$ epilayers. CL line scans crossing the identified BSFs allow us to disentangle the I_1 BSF-related emission from the fluctuating NBE luminescence. After acquiring dozens of CL line scans from each sample, we compile a statistics of the I_1 BSF-associated transition energies (E_{BSF}) to clearly determine the energy range of the I_1 BSF-related luminescence line in m-plane $Zn_{1-x}Mg_xO$ films for $0 \leqslant x \leqslant 0.1$. Both the E_{BSF} and E_{NBE} values exhibit a linear dependence on the Mg content for the investigated $Zn_{1-x}Mg_xO$ films. From the I_1 BSF-related luminescence features, we roughly estimate the densities of I_1 BSFs in m-plane $Zn_{1-x}Mg_xO$ epilayers, which were found to be nearly independent on the Mg content x.

II. EXPERIMENT

m-plane $Zn_{1-x}Mg_xO$ ($0 \leqslant x \leqslant 0.1$) epilayers, with an average thickness of around 180 nm, were grown on γ-$LiAlO_2$ (100) substrates by metal organic chemical vapor deposition in a three-temperature-zone furnace. Zinc acetylacetonate hydrate [$Zn(C_5H_7O_2)_2 \cdot xH_2O$, Alfa Aesar, 98%] and magnesium acetylacetonate [$Mg(C_5H_7O_2)_2$, Aldrich, 98%] were used as Zn and Mg precursors, respectively. γ-$LiAlO_2$ (100) substrates were loaded into the high-temperature zone of the furnace, where the growth temperature was maintained at 650° C. The Zn and Mg precursors were placed in two Pyrex glass containers and were loaded into the two low-temperature zones of the furnace. The vaporizing temperature of the Zn precursor was fixed at 121° C. Different Mg contents x of the $Zn_{1-x}Mg_xO$ epilayers were tailored via controlling the vaporizing temperatures of the Mg sources in the range between 180 and 205° C. The growth pressure was maintained at 200 Torr. More details of the growth conditions have been described elsewhere [11,18]. The Mg content of m-plane $Zn_{1-x}Mg_xO$ epilayers was determined by energy dispersive x-ray (EDX) spectroscopy attached to a scanning electron microscope (SEM).

Spectrally and spatially resolved luminescence measurements of the m-plane $Zn_{1-x}Mg_xO$ epilayers have been performed by CL spectroscopy and imaging in an SEM equipped with a Gatan monoCL4 system at 7 K using a He-cooling stage. Secondary electron (SE) and monochromatic CL images were acquired simultaneously, showing the corresponding spatial origin of the CL in the m-plane $Zn_{1-x}Mg_xO$ epilayers. CL spectra along a line (line scans) were recorded using a charge-coupled device detector. By utilizing Monte Carlo simulations [41] of the electron scattering trajectories within the m-plane $Zn_{1-x}Mg_xO$ epilayers (data not shown), we confirmed that, for a value of the electron beam energy of 3 keV, more than 90% of the electron energy is dissipated within the epilayers. As a result, all spatial and spectral CL measurements in the present work were performed using an electron acceleration voltage of 3 kV to avoid any signal contribution from the substrate. A statistical analysis of the E_{BSF} values in the $Zn_{1-x}Mg_xO$ epilayers was performed by collecting dozens of CL line scans from each sample and by fitting the corresponding CL spectra using Gaussian functions if necessary. From the statistical results, we were able to distinguish the significant contributions of single I_1 BSFs from those which experience energy shifts caused by electronic coupling within bundles of I_1 BSFs and/or by fluctuations of the Mg composition.

III. RESULTS AND DISCUSSION

A. Quantum-well model of the I_1 basal-plane stacking fault in ZnO

To verify the assumption that the luminescence line centered at a spectral position of about 3.32 eV in ZnO is related to the recombination of excitons captured within a QW formed by an I_1 BSF, we calculate the emission energy of an exciton confined into such a QW. In these simulations, an I_1 BSF consists of a 0.69-nm-thick (1.5 times the lattice constant of ZB ZnO) type-II QW of ZB ZnO in WZ ZnO. Electrons are confined in the ZB QW. The CB as well as the VB offset at the interface between the ZB and WZ phases are taken from Ref. [23], and the energy gap of ZB ZnO is assumed to be 3.324 eV, all of which have already been discussed

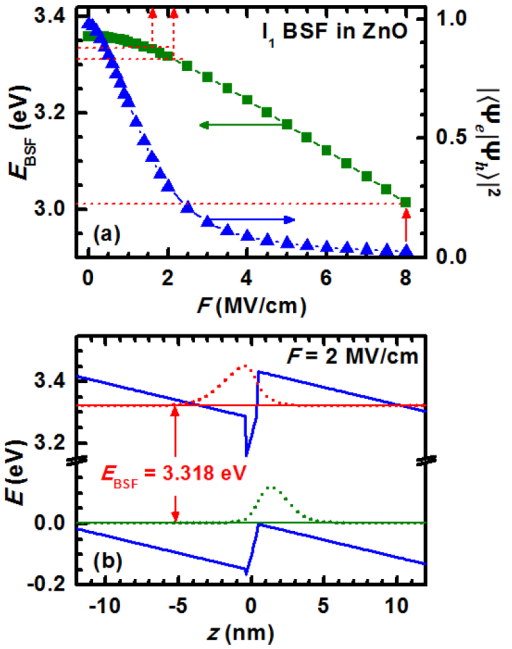

FIG. 1. (a) Transition energy E_{BSF} (squares) and modulus squared of the overlap integral (triangles), $|\langle\Psi_e|\Psi_h\rangle|^2$, as a function of the spontaneous polarization-related electric-field strength (F) for an exciton bound to an I_1 BSF in ZnO. The vertical solid arrow indicates the value of F expected from the spontaneous polarization of WZ ZnO. The vertical dashed arrows mark the energy range, within which I_1 BSF-related emission has been observed experimentally. (b) Band profile as well as electron and hole wave functions for $F = 2\,\mathrm{MV/cm}$.

in the Introduction. We assume that the electron and hole effective masses are $0.24m_0$ and $0.59m_0$ [42], respectively, in both the WZ and ZB phases of ZnO. In addition to the Coulomb interaction between the electron and the hole, we account for the built-in electric fields (F) that arise from the discontinuity of the polarization fields at the interfaces between WZ and ZB ZnO. The value of F has been varied between 0 and 8 MV/cm. The latter value of F corresponds roughly to that expected for the spontaneous polarization of WZ ZnO (-0.05 C/m^2) in the absence of any electric-field screening.

To solve the Schrödinger equation, we use the variational method described in Ref. [43]. The trial wave function for the exciton is two dimensional, and the variational parameter is the in-plane Bohr radius of the exciton. Figure 1(a) shows the resulting exciton transition energy E_{BSF} (squares) and the modulus squared of the overlap integral $|\langle\Psi_e|\Psi_h\rangle|^2$ of the electron (Ψ_e) and hole (Ψ_h) wave functions (triangles) as a function of F. When the discontinuity of the polarization field at the interface between WZ and ZB ZnO is neglected, the values of E_{BSF} and $|\langle\Psi_e|\Psi_h\rangle|^2$ are 3.360 eV and 0.98, respectively. A value of $|\langle\Psi_e|\Psi_h\rangle|^2$ close to unity indicates that, despite the type-II band alignment between WZ and ZB ZnO, an exciton confined in an I_1 BSF exhibits a large radiative efficiency. This finding arises from the fact that (i) the thickness of the ZB segment related to an I_1 BSF is smaller than the Bohr radius of the exciton in bulk ZnO and (ii) the CB and VB offsets are small, which allows for a significant spreading of the electron and the hole wave functions into the WZ and ZB phases, respectively. With increasing values of F, the values of E_{BSF} and $|\langle\Psi_e|\Psi_h\rangle|^2$ decrease, reaching 3.014 eV and 0.026 at $F = 8$ MV/cm [cf. solid arrow in Fig. 1(a)], respectively. According to this result, the I_1 BSF-related luminescence lines are expected to appear at a spectral position close to 3.014 eV, if the polarization-related electrical field is not screened. However, according to experiments performed by various authors [25–31], the I_1 BSF-related luminescence line appears systematically within a rather narrow energy range between about 3.310 and 3.335 eV. Comparing the calculated dependence of E_{BSF} on F [Fig. 1(a)] with the experimentally found values of E_{BSF}, we have to assume that the effective electrical field of the I_1 BSF-related QW is much smaller than expected and amounts actually to about 2 MV/cm [cf. vertical dashed arrows in Fig. 1(a)].

In Fig. 1(b), we show the band structure of the I_1 BSF for $F = 2$ MV/cm with the corresponding electron and hole wave functions as well as energy levels resulting in $E_{\mathrm{BSF}} = 3.318$ eV, which corresponds to the experimentally observed energy range. According to this band structure, both the electron and the hole are localized within trianglelike potential wells including the BSF, and $|\langle\Psi_e|\Psi_h\rangle|^2$ exhibits a value of about 0.3, which is consistent with the experimentally observed efficient excitonic emission originating from the BSF plane, as has been shown by spatially resolved CL spectroscopy [28].

The remaining questions are (i) Why is the electrical field by a factor of 4 smaller than expected for a spontaneous polarization of about -0.05 C/m^2? (ii) If we consider electric-field screening, why does the I_1 BSF-related emission appear always within a rather narrow energy range at about 3.32 eV regardless of the origin of the sample and of the used excitation conditions?

Apparently, we are facing an efficient screening of the polarization field in the I_1 BSF-related QWs. Generally, electric-field screening is attributed to free carriers due to doping or excitation. In contrast, for electric-field screening by free carriers, we would expect a large variation of E_{BSF} for different samples and different research groups depending on the respective doping and excitation conditions. However, this is not the case, but instead the available values of E_{BSF} in the literature [25,26,29–31] and our own experimentally obtained E_{BSF} values (Ref. [28] and this work) vary only by about 25 meV around 3.32 eV. Thus, screening of the polarization-related electric field by free carriers can hardly explain the observed experimental results.

A similar issue has been found for I_1 BSFs in GaN. Lähnemann *et al.* [36] performed CL line scans crossing E-type, I_2-type, and I_1-type BSFs in GaN microcrystals. While the electron beam is approaching a BSF during such a line scan, the authors observe a clear blueshift for the CL spectrum of the E and I_2 BSF due to a screening of the polarization field by the excited carriers, the concentration of which increases with decreasing distance with respect to the BSF. For the I_1 BSF, however, a corresponding blueshift can hardly be observed. We performed similar CL line scan experiments of the I_1 BSF in ZnO with the same result (Ref. [28] and this work).

The systematic observation of a built-in electrical field with a value smaller than that expected value in thin QWs related to I_1 BSFs indicates a more fundamental screening mechanism,

which should be the same for samples of different origin and which does not depend on the free-carrier concentration. Such a common screening mechanism for very thin c-plane QWs in polar semiconductors has been discussed by Corfdir and Lefebvre [43], who considered that, according to calculations performed by Bernardini and Fiorentini [44], the charge densities at both interfaces of polar QWs exhibit a spatial extent of about two monolayers along the confinement direction. Hence, for I_1 BSF-related QWs with a well width of three monolayers, we have to take into account an overlap of the opposite charges of the two interface planes. This charge overlap can at least partially screen the polarization-related built-in field of such narrow QWs and is independent of the free-carrier concentration. We believe that this fundamental screening mechanism of very thin QWs is responsible for the significant screening of the electrical field of I_1 BSFs in ZnO and GaN, leading to the observation of a relatively fixed value of E_{BSF} for samples with varying doping concentrations and excitation conditions.

Concerning the 25-meV variation of E_{BSF} in ZnO from sample to sample or the dependence on the excitation position within a given sample, at least two effects have to be considered. First, there can still be a different degree of screening of the remaining built-in field by free carriers due to different doping or excitation conditions. Second, as shown by Corfdir *et al.* [45] for GaN, excitons localized within the plane of a BSF can additionally be localized at donors, which are situated in the vicinity of this BSF. Since the localization energy of excitons on donors depends on the exact distance between the donor and the BSF, this additional localization leads to a broadening of the emission spectra and to some variation in the value of E_{BSF}. Note that the localization of excitons by donors distributed in the vicinity of the BSF plane is consistent with the S-shape temperature dependence of E_{BSF} reported by Yang *et al.* [27] in ZnO epitaxial films grown by atomic layer deposition.

B. Luminescence spectra of $Zn_{1-x}Mg_xO$ related to I_1 basal-plane stacking faults

Figure 2 shows typical normalized CL spectra of $Zn_{1-x}Mg_xO$ films acquired from a 4.3×4.3-μm^2 large sample region at 7 K. As shown in Fig. 2(a), two distinct peaks are observed in the CL spectrum of the ZnO film. The peak centered at 3.379 eV is assigned to the donor-bound excitons (D^0X), while the one at 3.32 eV is attributed to the I_1 BSF-related emission as described above. Figure 2(b) depicts the CL spectrum of the $Zn_{0.97}Mg_{0.03}O$ film. A symmetric CL line with a significant shoulder at its lower energy side is observed. After fitting the CL spectrum by two Gaussian functions, two lines are obtained as shown in Fig. 2(b). We assign the CL line centered at 3.416 eV to the NBE emission of the $Zn_{0.97}Mg_{0.03}O$ film. The NBE CL line is slightly broadened and shifted toward higher energies as compared to that of ZnO shown in Fig. 2(a). This result indicates a successful alloying by means of substituting Mg atoms for Zn ones.

We exclude the donor-acceptor-pair transition in $Zn_{1-x}Mg_xO$ as a possible origin of the CL line centered at 3.363 eV in Fig. 2(b), since such an emission line was found at energies which are 140 and 135 meV smaller than E_{NBE} in ZnO and $Zn_{0.85}Mg_{0.15}O$, respectively [27,40]. In cntrast, the difference between E_{NBE} and the energy of the additional peak observed in Fig. 2(b) is only 48 meV. This value is close to the energy difference $E_{NBE} - E_{BSF}$ measured for ZnO in Fig. 2(a) and agrees well with the work of Chia *et al.* [12], which reported an energy separation of 50 meV between the NBE emission and a stacking fault-related (e, A^0) transition for $Zn_{1-x}Mg_xO$ films with $x \leqslant 0.12$. Following the model described above, we assign the CL line centered at 3.363 eV to excitons confined in a type-II QW formed by I_1 BSFs in the $Zn_{0.97}Mg_{0.03}O$ film.

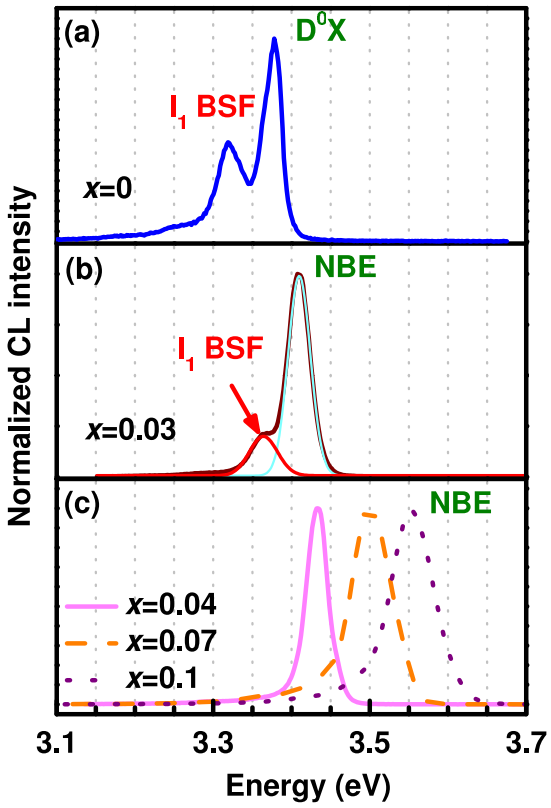

FIG. 2. Typical normalized CL spectra of m-plane $Zn_{1-x}Mg_xO$ epilayers acquired at 7 K for (a) $x = 0$, (b) $x = 0.03$, and (c) $0.04 \leqslant x \leqslant 0.1$. The NBE luminescence of ZnO is attributed to donor-bound excitons (D^0X), while that of $Zn_{1-x}Mg_xO$ ($0.03 \leqslant x \leqslant 0.1$) arises from the recombination of excitons bound to potential minima caused by spatial composition variations and/or to donor states.

With the Mg composition increasing to 0.04, 0.07, and 0.1 [cf. Fig. 2(c)], the measured CL line blueshifts and broadens. A tail on the low-energy side of the CL band is observed, but no I_1 BSF-related emission can be resolved anymore. The broadening of the CL line with increasing Mg content is caused by local composition fluctuations. Thus, the CL or PL spectra, for which a certain region is excited (as is the case in Fig. 2), represent an average over such composition fluctuations and thus become broader. The E_{NBE} values of the $Zn_{1-x}Mg_xO$ films obtained from Fig. 2 are summarized in Table I.

In order to perform a local measurement of the I_1 BSF-related optical emission that is less affected by the spatial composition variations, we first have to determine the positions of these defects. For this purpose, we have recorded

TABLE I. List of the NBE-related emission energies from spatially integrated CL spectra in Fig. 2, I_1 BSF-related emission energies and full width at half maximum (FWHM) of the emission line obtained from the statistical results of the CL line scans in Fig. 6, and density of I_1 BSFs in $Zn_{1-x}Mg_xO$ epilayers estimated from monochromatic CL maps.

Mg content x	E_{NBE} (eV)	E_{BSF} (eV)	FWHM (meV)	density of I_1 BSFs (cm^{-1})
0	3.379	3.325	6.95	8.1×10^4
0.03	3.416	3.365	8.20	4.4×10^4
0.04	3.433	3.383	8.22	3.7×10^4
0.07	3.503	3.451	13.76	6.0×10^4
0.1	3.553	3.502	23.75	1.3×10^5

monochromatic CL maps setting the CL detection energy to E_{NBE} and to $E_{NBE} - 50$ meV, assuming that the CL features of the latter one represent the positions of the I_1 BSFs.

Figure 3 shows typical bichromatic CL maps of the ZnO and $Zn_{0.93}Mg_{0.07}O$ films acquired for CL detection energies, which correspond to the respective values of E_{NBE} and E_{BSF}. The CL maps are superimposed on the corresponding SE images. The CL detection energies are indicated by the respective colors in Fig. 3. The surface of both samples exhibits particular stripelike features with their longitudinal axis parallel to the c direction, which are typical for m-plane $Zn_{1-x}Mg_xO$ films [18]. While at E_{NBE} the CL intensity distribution covers almost the entire mapped region, the CL intensity distribution for the detection energy representing E_{BSF} consists of distinct features, which exhibit an elongated shape perpendicular to the c direction and which are terminated at the borders of the morphological stripes visible at the surface. For GaN, it is well known that BSFs can be terminated by partial dislocations and/or prismatic stacking faults [46].

Since it is expected that, at the borders between the stripelike surface features, the layer contains extended defects such as dislocations as a result of the coalescence of neighboring stripes, we believe that for our ZnO and $Zn_{1-x}Mg_xO$ epilayers the termination of the BSFs is triggered by such defects and occurs via the formation of partial dislocations and/or prismatic stacking faults. Accordingly, the BSF-related

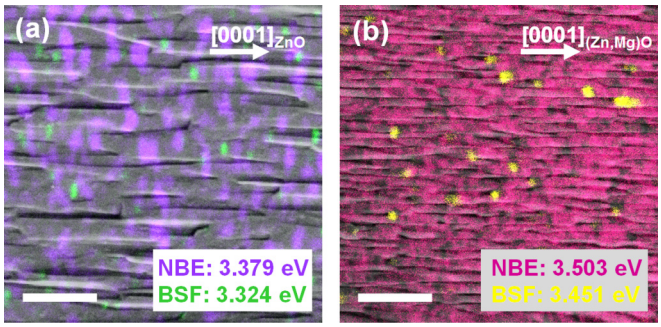

FIG. 3. Typical color-coded bichromatic CL intensity maps acquired at 7 K and superimposed on the corresponding SE micrographs of (a) a ZnO and (b) a $Zn_{0.93}Mg_{0.07}O$ epilayer for a CL detection energy corresponding to the NBE- and I_1 BSF-related emission energies denoted in the respective colors. The scale bars in both images correspond to 1 μm.

emission of ZnO and $Zn_{1-x}Mg_xO$ epilayers is confined within the crystalline stripes as shown in Fig. 3. Note that the distinct features visible in the CL maps for the BSFs emission indicate the position of the I_1 BSFs, which allows us to perform spatially resolved CL measurements in the form of line scans crossing the positions of these I_1 BSFs.

Figure 4 shows three typical CL line scans across I_1 BSFs in $Zn_{1-x}Mg_xO$ films with $x = 0$, 0.03, and 0.07. Each CL line scan consists of more than 50 individual spectra and is shown as a two-dimensional plot with the intensity color coded. The intensity of the NBE emission varies along the line scans due to an inhomogeneous distribution of nonradiative defects in the films. The fluctuations in the peak energy of the NBE emission along the line also increase with increasing Mg content. Despite these fluctuations, the I_1 BSF-related emission is clearly resolved even for $x = 0.07$, which was not possible in the corresponding integrated CL spectrum shown in Fig. 2(c).

For a more convincing demonstration, we compare the CL spectra of the ZnO with the ones of $Zn_{0.93}Mg_{0.07}O$ films picked up from the regions marked by the rectangles in Figs. 4(a) and 4(c), which are shown in Figs. 5(a) and 5(b), respectively. The steps between two spots (spectra) amount to 30 nm in Fig. 5(a) and 20 nm in Fig. 5(b). The CL spectra showing a prominent transition related to I_1 BSF are displayed by the blue curves. The red curves highlight the spectra for which the electron beam excites the I_1 BSF position directly or in close proximity. Clearly, the I_1 BSF-related emission line can be well distinguished from the NBE emission, not only for ZnO, but also for $Zn_{0.93}Mg_{0.07}O$. Moreover, the free exciton (FX) emission for the NBE emission of the ZnO film shown in Fig. 5(a) can be observed as a shoulder on the high-energy side of the D^0X emission, which can barely be recognized in the integrated CL spectrum acquired over a larger area [cf. Fig. 2(a)]. Consequently, a CL line scan with the electron beam in spot mode enables us to determine the spectral position of the transition related to I_1 BSFs in $Zn_{1-x}Mg_xO$ films more precisely than measurements averaging over a certain region. This finding results from the local carrier excitation, which allows for the minimization of the line broadening caused by Mg composition fluctuations. Furthermore, the CL line scans in Fig. 4 and the line scan spectra in Figs. 5(a) and 5(b) show exemplarily the complementary appearance and disappearance of the I_1 BSF-related and NBE emission, respectively, when the electron beam is crossing the BSF position.

The sketch in Fig. 5(c) summarizes the scenario of carrier excitation and relaxation in $Zn_{1-x}Mg_xO$ layers containing an I_1 BSF. Electrons and holes excited by the high-energy electron beam relax down to the CB and VB edge, respectively, and subsequently form free excitons (FXs). At low temperatures, FXs can further relax down to potential minima arising from composition fluctuations and/or can be captured by donor states (D^0X) both forming bound excitons (BXs). The radiative recombination of BX results in the NBE emission line, the broadening of which increases with increasing Mg content due to composition fluctuations. Electrons directly excited at the position of an I_1 BSF or that have diffused to this defect are efficiently captured by the ZB QW and attract holes to form excitons, following the picture described above for ZnO. Alternatively, excitons generated away from the

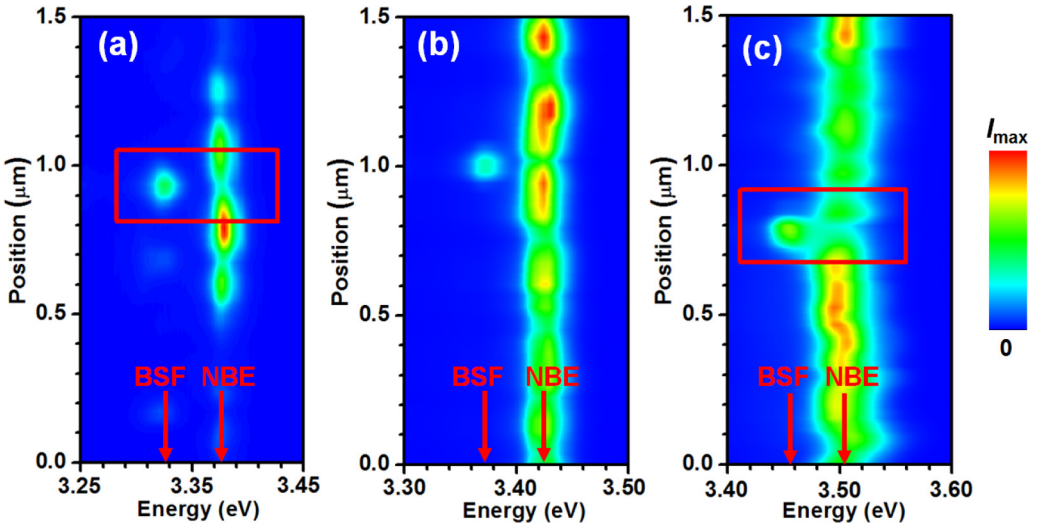

FIG. 4. CL spectral line scans across a region of $Zn_{1-x}Mg_xO$ films containing I_1 BSFs, where the intensity is color coded for (a) $x = 0$, (b) $x = 0.03$, and (c) $x = 0.07$. The rectangles in (a) and (c) mark the regions for which the corresponding CL spectra are plotted in Figs. 5(a) and 5(b), respectively. The arrows indicate E_{BSF} and E_{NBE}. I_{max} indicates the maximum CL intensity detected for each line scan.

I_1 BSF may also diffuse to and be captured by the planar defect [47]. For $x \neq 0$, the recombination of the BX bound to the I_1 BSF is also broadened due to composition variations leading to an increasing overlap of the NBE- and I_1 BSF-related luminescence lines, when the Mg content becomes larger.

Besides composition variations, several other factors can lead to a shift and/or broadening of the I_1 BSF-related emission line as summarized in Ref. [36] for GaN. These are for example a bundling of BSFs, an energy coupling with point defects, a strain-induced energy shift, and an excitation density-dependent partial screening of the polarization field.

Considering the above discussed mechanisms leading to variations of the transition energy of excitons bound to I_1 BSFs, a statistics of these transition energies is necessary in order to reliably determine the I_1 BSF-related emission energies of $Zn_{1-x}Mg_xO$ films as a function of x. Therefore, we have recorded for each $Zn_{1-x}Mg_xO$ sample investigated in this study dozens of CL line scans with the electron beam in spot mode exactly crossing a region containing I_1 BSF-related CL features in a similar way as shown in Fig. 4. Similar experiments to distinguish three types of BSFs and to disentangle polarization field screening effects on the BSF-related luminescence lines in GaN have been carried out in Refs. [35] and [36]. Note that the factors being responsible for energy variations of the I_1 BSF-related emission line such as bundling of BSFs, coupling with adjacent point defects, spontaneous polarization effects, and composition fluctuation-induced broadening effects are all included in our detected E_{BSF} values of $Zn_{1-x}Mg_xO$ films, where these factors can hardly be discussed independently.

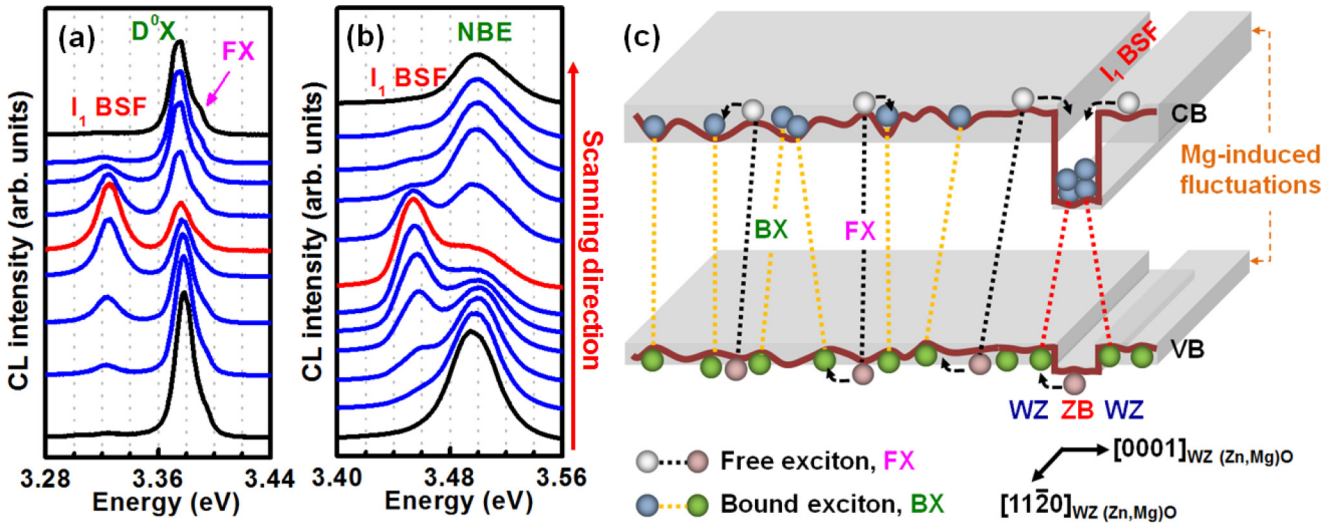

FIG. 5. CL spectra associated with the I_1 BSF-related emission of $Zn_{1-x}Mg_xO$ epilayers for (a) $x = 0$ and (b) $x = 0.07$ selected from the region marked by the rectangles in Figs. 4(a) and 4(c), respectively. (c) Simplified sketch of the band profile of $Zn_{1-x}Mg_xO$ epilayers containing an I_1 BSF without taking into account the spontaneous-polarization effect. Potential fluctuations caused by spatial variations of the Mg content are denoted by grey regions as well as by the wavy VB and CB edges.

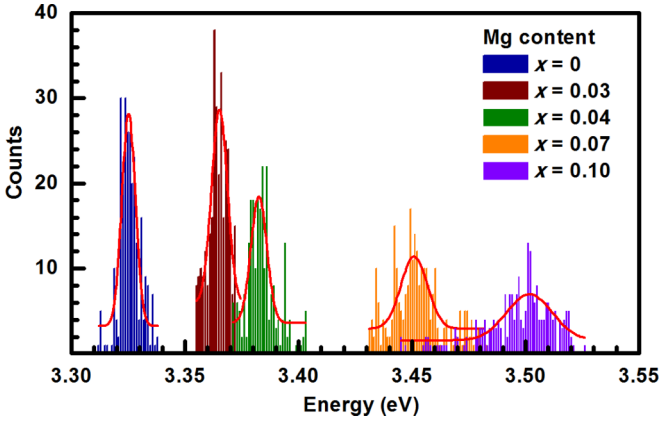

FIG. 6. Statistical histograms of the I_1 BSF-related emission energies of $Zn_{1-x}Mg_xO$ epilayers studied in this work. Each histogram was evaluated from dozens of CL line scans across I_1 BSFs of each sample. The Gaussian distributions (solid lines) show five distinct peaks centered at 3.325, 3.365, 3.383, 3.451, and 3.502 eV for the $Zn_{1-x}Mg_xO$ films with $x = 0$, 0.03, 0.04, 0.07, and 0.1, respectively.

Figure 6 shows statistical histograms of the E_{BSF} values for all investigated $Zn_{1-x}Mg_xO$ films. We have applied Gaussian functions to deconvolute the CL spectra if there is a strong overlap between the NBE and I_1 BSF peaks as for example for the spectrum highlighted in red in Fig. 5(b). The histograms in Fig. 6 have also been fitted by Gaussian distributions, yielding that the I_1 BSF transition energies in $Zn_{1-x}Mg_xO$ with $x =$ 0, 0.03, 0.04, 0.07, and 0.1 are 3.325, 3.365, 3.383, 3.451, and 3.502 eV, respectively. In Fig. 6, we clearly observe the expected blueshift and broadening of the energy distribution of the I_1 BSF-related emission with increasing Mg content x. For the five investigated $Zn_{1-x}Mg_xO$ samples, Table I summarizes the E_{BSF} values and the corresponding values of the full width at half maximum (FWHM) derived from the statistics as shown in Fig. 6.

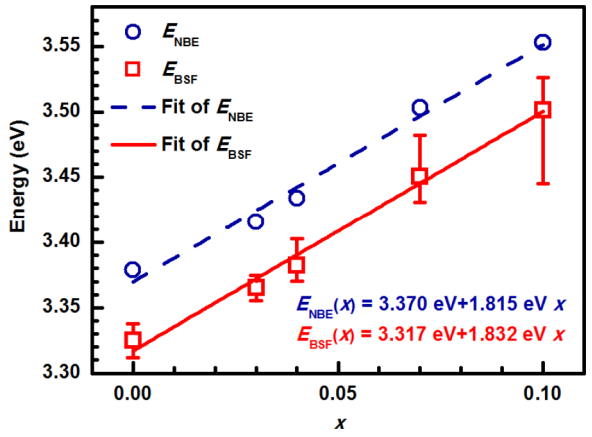

FIG. 7. Emission energies of the NBE transition (E_{NBE}) and related to the I_1 BSF (E_{BSF}) of $Zn_{1-x}Mg_xO$ films as a function of Mg content x. The vertical bars show the respective lowest and highest observed E_{BSF} values derived from the statistical histograms in Fig. 6. The dashed and solid lines indicate linear fits to the data points without taking into account the vertical bars.

Figure 7 shows the values of E_{NBE} and E_{BSF} of the five $Zn_{1-x}Mg_xO$ layers listed in Table I as a function of the Mg content x, where the latter has been determined by EDX. As expected, both emission energies exhibit a linear dependence on the Mg content for

$$E_{NBE}(x) = 3.370\ \text{eV} + 1.815\ \text{eV}x, \quad (1)$$

$$E_{BSF}(x) = 3.317\ \text{eV} + 1.832\ \text{eV}x. \quad (2)$$

The slope of $E_{BSF}(x)$ has been determined from the most probable energies for a single BSF. If we include the least probable values in the determination of the slope, we obtain values in the range 1.4–2.0. The values of the slopes of $E_{NBE}(x)$ and $E_{BSF}(x)$ given in Eqs. (1) and (2), respectively, are very similar, indicating that the values of E_{NBE} and E_{BSF} of $Zn_{1-x}Mg_xO$ films exhibit an almost parallel increase with increasing Mg content for the considered values of x.

Regarding the ZB phase of $Zn_{1-x}Mg_xO$ alloys, experimental results on the optical properties are not available so far, since the ZB structure is thermodynamically unstable under ambient conditions. Recently, Rashid *et al.* [48] have applied first-principle calculations to study the electronic and optical properties of ZB $Zn_{1-x}Mg_xO$ and obtained that the increase in the energy gap with increasing x is similar to that of WZ $Zn_{1-x}Mg_xO$. In their report, the VB maximum (VBM) of ZB $Zn_{1-x}Mg_xO$, occupied by the oxygen $2p$ state, is in fact less affected by Mg alloying. As a result, the energy gap increase of ZB $Zn_{1-x}Mg_xO$ with x is mainly ascribed to the fact that the CB moves away from the Fermi level.

Also, Hu *et al.* [49] have reported that the CB minimum (CBM) and the VBM determined by zinc $4s$ and oxygen $2p$ states, respectively, contribute to the observed energy gap of WZ ZnO. After alloying with Mg, the CBM of $Zn_{1-x}Mg_xO$ becomes dominated by zinc $4s$ and magnesium $2p$ hybrid states, while the VBM remains dominated by oxygen $2p$ states. In addition, Chang *et al.* [50] have theoretically demonstrated an Mg-induced enhancement of the localization of the oxygen $2p$ state in WZ $Zn_{1-x}Mg_xO$. As a result, the Mg-dependent energy gap broadening of WZ $Zn_{1-x}Mg_xO$ may be caused by a CBM shift toward higher energy levels, whereas the VBM remains nearly unchanged. Consequently, the observed linear dependencies of E_{NBE} and E_{BSF} on the Mg content exhibit an almost identical slope, because the CBMs of the WZ and the ZB $Zn_{1-x}Mg_xO$ shift to higher energies in the same way, while the corresponding VBMs are nearly unaffected. Thus, an energy difference of about 50 meV between the NBE and the BSF-related emission energies of the $Zn_{1-x}Mg_xO$ layer is always observed both in Ref. [12] and in the present study.

Taking advantage of the established dependence of the I_1 BSF-related emission energy on the Mg content, it is possible to determine the densities of I_1 BSFs in the $Zn_{1-x}Mg_xO$ films by CL experiments. We have acquired monochromatic CL maps from all $Zn_{1-x}Mg_xO$ samples at their corresponding I_1 BSF-related CL energies in the same way as shown in Fig. 3. The densities of I_1 BSFs derived from such CL maps are shown in Table I and are on the order of 10^4–10^5 cm^{-1} for all investigated samples. However, the estimated density of I_1 BSFs does not show any significant dependence on the Mg content.

Previously, we estimated the density of I_1 BSFs in an 850-nm-thick *m*-plane ZnO film by TEM investigations to be about 10^5 cm^{-1} [21]. Utilizing monochromatic CL imaging, the density of I_1 BSFs of the same ZnO film was estimated to be 2.5×10^4 cm^{-1} [28]. Despite the deviation between the values of the density derived by TEM and CL, which is mainly due to different spatial resolution capabilities of TEM and SEM-CL, the latter technique is a reliable and promising method for the identification of BSFs and for the estimation of their density in $Zn_{1-x}Mg_xO$ films without the need of sophisticated TEM investigations.

IV. CONCLUSIONS

We have calculated the energy of an exciton in an I_1 BSF in ZnO assuming that it acts as a type-II QW taking into account the built-in electric fields that arise from the discontinuity of the spontaneous polarization field between WZ and ZB ZnO. The resulting excitonic transition energy corresponds to the experimentally observed value only if we assume that the built-in electric fields are partially screened. We rule out that this partial screening could be due to free carriers trapped in the BSF plane. Instead, we propose that it is an intrinsic effect resulting from the spatial overlap between sheet charges at the QW interfaces.

We have observed NBE- and I_1 BSF-related optical emission in $Zn_{1-x}Mg_xO$ films. When CL spectra are acquired from a large region of the sample, the broadening of both the NBE and I_1 BSF emission lines caused by composition variations prevents the resolution of the individual transitions. We take advantage of bichromatic CL maps acquired at the NBE and I_1 BSF emission energies of $Zn_{1-x}Mg_xO$, which clearly show complementary features, to determine the position of I_1 BSFs enabling local CL line scans crossing the I_1 BSFs. By means of such locally excited CL spectra, we were able to disentangle the I_1 BSF-related optical emission from the NBE one for $Zn_{1-x}Mg_xO$ layers with $0 < x \leqslant 0.1$. We then established a linear correlation between the I_1 BSF-related emission energy and the Mg content, which offers an alternative and simplified way to study the properties of I_1 BSFs in $Zn_{1-x}Mg_xO$. Knowing the emission energy of I_1 BSFs with increasing x, it is possible to estimate the density of these defects by means of CL maps. We find that, for the $Zn_{1-x}Mg_xO$ epilayers investigated in this study, the density of I_1 BSFs does not depend on the Mg content.

ACKNOWLEDGMENTS

The authors would like to thank M. M. C. Chou for supplying $LiAlO_2$ substrates, Y. Takagaki for program design on data processing, and T. Flissikowski for a careful reading of the manuscript. W.H.L. is thankful for the support of "NSC-DAAD Sandwich Program, 2012 Spring" from the National Science Council (NSC) in Taiwan and the German Academic Exchange Service (DAAD) in Germany under the Grant No. 100-2911-I-006-016-2 as well as the "Postdoctoral Research Abroad Program" from the Ministry of Science and Technology (MOST) in Taiwan under Grant No. 104-2917-I-564-079. P.C. acknowledges funding from the Fonds National Suisse de la Recherche Scientifique through Project No. 161032.

[1] S. Chakrabarti and B. K. Dutta, J. Hazard. Mater. **112**, 269 (2004).
[2] W.-H. Lin, J.-J. Wu, M. M. C. Chou, Y.-M. Chang, and M. Yoshimura, J. Phys. Chem. C **118**, 19814 (2014).
[3] C.-T. Wu, W.-P. Liao, and J.-J. Wu, J. Mater. Chem. **21**, 2871 (2011).
[4] H.-W. Cho, W.-P. Liao, W.-H. Lin, M. Yoshimura, and J.-J. Wu, J. Power Sources **293**, 246 (2015).
[5] Q. Wan, Q. H. Li, Y. J. Chen, T. H. Wang, X. L. He, J. P. Li, and C. L. Lin, Appl. Phys. Lett. **84**, 3654 (2004).
[6] L. Guo, H. Zhang, D. X. Zhao, B. H. Li, Z. Z. Zhang, M. M. Jiang, and D. Z. Shen, Sensor Actuat. B: Chem. **166–167**, 12 (2012).
[7] X.-L. Guo, J.-H. Choi, H. Tabata, and T. Kawai, Jpn. J. Appl. Phys. **40**, L177 (2001).
[8] D. X. Zhao, Y. C. Liu, D. Z. Shen, Y. M. Lu, J. Y. Zhang, and X. W. Fan, J. Appl. Phys. **90**, 5561 (2001).
[9] S.-H. Park, K.-B. Kim, S.-Y. Seo, S.-H. Kim, and S.-W. Han, J. Electron. Mater. **35**, 1680 (2006).
[10] J. W. Chiou, H. M. Tsai, C. W. Pao, F. Z. Chien, W. F. Pong, C. W. Chen, M.-H. Tsai, J. J. Wu, C. H. Ko, H. H. Chiang, H.-J. Lin, J. F. Lee, and J.-H. Guo, J. Appl. Phys. **104**, 013709 (2008).
[11] W.-H. Lin, M. M. C. Chou, and J.-J. Wu, J. Electrochem. Soc. **158**, D28 (2011).
[12] C. H. Chia, Y. F. Tsai, and S. J. Tzou, J. Alloys Compd. **622**, 979 (2015).
[13] P. Waltereit, O. Brandt, A. Trampert, H. T. Grahn, J. Menniger, M. Ramsteiner, M. Reiche, and K. H. Ploog, Nature (London) **406**, 865 (2000).
[14] T. Makino, A. Ohtomo, C. H. Chia, Y. Segawa, H. Koinuma, and M. Kawasaki, Physica E **21**, 671 (2004).
[15] Y.-T. Ho, W.-L. Wang, C.-Y. Peng, M.-H. Liang, J.-S. Tian, C.-W. Lin, and L. Chang, Appl. Phys. Lett. **93**, 121911 (2008).
[16] E. Cagin, J. Yang, W. Wang, J. D. Phillips, S. K. Hong, J. W. Lee, and J. Y. Lee, Appl. Phys. Lett. **92**, 233505 (2008).
[17] M. M. C. Chou, L. Chang, D.-R. Hang, C. L. Chen, D.-S. Chang, and C.-A. Li, Cryst. Growth Des. **9**, 2073 (2009).
[18] W.-H. Lin, J.-J. Wu, M. M. C. Chou, and L. Chang, Cryst. Growth Des. **9**, 3301 (2009).
[19] L. Béaur, T. Bretagnon, B. Gil, A. Kavokin, T. Guillet, C. Brimont, D. Tainoff, M. Teisseire, and J.-M. Chauveau, Phys. Rev. B **84**, 165312 (2011).
[20] P. Vennéguès, J. M. Chauveau, M. Korytov, C. Deparis, J. Zuniga-Perez, and C. Morhain, J. Appl. Phys. **103**, 083525 (2008).
[21] T.-H. Huang, W.-H. Lin, T. Yan, J.-J. Wu, L. Chang, M. M. C. Chou, U. Jahn, and K. H. Ploog, ECS J. Solid State Sci. Technol. **2**, P338 (2013).
[22] P. Vennéguès, J. M. Chauveau, Z. Bougrioua, T. Zhu, D. Martin, and N. Grandjean, J. Appl. Phys. **112**, 113518 (2012).
[23] Y. Yan, G. M. Dalpian, M. M. Al-Jassim, and S.-H. Wei, Phys. Rev. B **70**, 193206 (2004).

[24] M. Schirra, R. Schneider, A. Reiser, G. M. Prinz, M. Feneberg, J. Biskupek, U. Kaiser, C. E. Krill, K. Thonke, and R. Sauer, Phys. Rev. B **77**, 125215 (2008).
[25] L. Lazzarini, G. Salviati, F. Fabbri, M. Z. Zha, D. Calestani, A. Zappettini, T. Sekiguchi, and B. Dierre, ACS Nano **3**, 3158 (2009).
[26] K. Thonke, M. Schirra, R. Schneider, A. Reiser, G. M. Prinz, M. Feneberg, R. Sauer, J. Biskupek, and U. Kaiser, Phys. Status Solidi B **247**, 1464 (2010).
[27] S. Yang, C. C. Kuo, W.-R. Liu, B. H. Lin, H.-C. Hsu, C.-H. Hsu, and W. F. Hsieh, Appl. Phys. Lett. **100**, 101907 (2012).
[28] W.-H. Lin, U. Jahn, H. T. Grahn, L. Chang, M. M. C. Chou, and J.-J. Wu, Appl. Phys. Express **6**, 061101 (2013).
[29] V. Khranovskyy, A. M. Glushenkov, Y. Chen, A. Khalid, H. Zhang, L. Hultman, B. Monemar, and R. Yakimova, Nanotechnology **24**, 215202 (2013).
[30] S. Yang, H. C. Hsu, W.-R. Liu, B. H. Lin, C. C. Kuo, C.-H. Hsu, M. O. Eriksson, P. O. Holtz, and W. F. Hsieh, Appl. Phys. Lett. **105**, 011106 (2014).
[31] V. Khranovskyy, M. O. Eriksson, G. Z. Radnoczi, A. Khalid, H. Zhang, P. O. Holtz, L. Hultman, and R. Yakimova, Physica B **439**, 50 (2014).
[32] Z. N. Urgessa, J. R. Botha, M. O. Eriksson, C. M. Mbulanga, S. R. Dobson, S. R. Tankio Djiokap, K. F. Karlsson, V. Khranovskyy, R. Yakimova, and P.-O. Holtz, J. Appl. Phys. **116**, 123506 (2014).
[33] Y. T. Rebane, Y. G. Shreter, and M. Albrecht, Phys. Status Solidi A **164**, 141 (1997).
[34] B. J. Skromme, L. Chen, M. K. Mikhov, H. Yamane, M. Aoki, and F. J. Disalvo, Mater. Sci. Forum **457–460**, 1613 (2004).
[35] J. Lähnemann, O. Brandt, U. Jahn, C. Pfüller, C. Roder, P. Dogan, F. Grosse, A. Belabbes, F. Bechstedt, A. Trampert, and L. Geelhaar, Phys. Rev. B **86**, 081302(R) (2012).
[36] J. Lähnemann, U. Jahn, O. Brandt, T. Flissikowski, P. Dogan, and H. T. Grahn, J. Phys. D: Appl. Phys. **47**, 423001 (2014).
[37] S.-K. Kim, S.-Y. Jeong, and C.-R. Cho, Appl. Phys. Lett. **82**, 562 (2003).
[38] F. Bernardini, V. Fiorentini, and D. Vanderbilt, Phys. Rev. B **56**, R10024(R) (1997).
[39] B. Laumer, T. A. Wassner, F. Schuster, M. Stutzmann, J. Schörmann, M. Rohnke, A. Chernikov, V. Bornwasser, M. Koch, S. Chatterjee, and M. Eickhoff, J. Appl. Phys. **110**, 093513 (2011).
[40] M. M. Morshed, Z. Zuo, J. Huang, J.-G. Zheng, Q. Lin, X. Q. Yan, and J. L. Liu, Appl. Phys. A **117**, 1467 (2014).
[41] D. Drouin, A. R. Couture, D. Joly, X. Tastet, V. Aimez, and R. Gauvin, Scanning **29**, 92 (2007).
[42] W. R. L. Lambrecht, A. V. Rodina, S. Limpijumnong, B. Segall, and B. K. Meyer, Phys. Rev. B **65**, 075207 (2002).
[43] P. Corfdir and P. Lefebvre, J. Appl. Phys. **112**, 053512 (2012).
[44] F. Bernardini and V. Fiorentini, Phys. Rev. B **57**, R9427(R) (1998).
[45] P. Corfdir, P. Lefebvre, J. Ristić, J.-D. Ganière, and B. Deveaud-Plédran, Phys. Rev. B **80**, 153309 (2009).
[46] R. Liu, A. Bell, F. A. Ponce, C. Q. Chen, J. W. Yang, and M. A. Khan, Appl. Phys. Lett. **86**, 021908 (2005).
[47] P. Corfdir, J. Ristić, P. Lefebvre, T. Zhu, D. Martin, A. Dussaigne, J. D. Ganière, N. Grandjean, and B. Deveaud-Plédran, Appl. Phys. Lett. **94**, 201115 (2009).
[48] M. Rashid, F. Hussain, M. Imran, G. S. Abo, S. A. Ahmad, and Y. P. Feng, Mater. Sci. Semicon. Process. **18**, 114 (2014).
[49] Y. H. Hu, B. Cai, Z. Y. Hu, Y. L. Liu, S. L. Zhang, and H. B. Zeng, Curr. Appl. Phys. **15**, 423 (2015).
[50] Y.-S. Chang, C.-T. Chien, C.-W. Chen, T.-Y. Chu, H.-H. Chiang, C.-H. Ku, J.-J. Wu, C.-S. Lin, L.-C. Chen, and K.-H. Chen, J. Appl. Phys. **101**, 033502 (2007).